

Atom probe crystallography

This review addresses new developments in the emerging area of “atom probe crystallography”, a materials characterization tool with the unique capacity to reveal both composition and crystallographic structure at the atomic scale. This information is crucial for the manipulation of microstructure for the design of both structural and functional materials with optimized mechanical, electric, optoelectronic, magnetic, or superconducting properties that will find application in, for example, nanoelectronics or energy generation. The ability to extract crystallographic information from 3D atomistic reconstruction has exciting potential synergies with modern modeling techniques, blending experimental and computational methods to extend our insight.

Baptiste Gault^{1,*}, Michael P. Moody², Julie M. Cairney^{3,4}, Simon P. Ringer^{3,4}

¹Department of Materials Science and Engineering, McMaster University, 1280 Main St W, Hamilton, Ontario L8S 4L8, Canada

²Department of Materials, University of Oxford, Parks Road, OX1 3PH, UK

³The Australian Centre for Microscopy and Microanalysis, The University of Sydney, Sydney, 2006, NSW, Australia

⁴School of Aerospace, Mechanical and Mechatronic Engineering, The University of Sydney, NSW 2006, Australia

*E-mail: gaultb@mcmaster.ca

Many new materials are now tailored at the nanoscale for specific applications. Hence, understanding the relationships that exist between the atomic-scale structure of a material system and its properties or performance is critical. The design of these materials and devices is underpinned by increasingly sophisticated microscopy techniques. However, in many cases continued development will require techniques capable of atomically-resolved three-dimensional characterization. Recent developments in electron microscopy towards this end have been well documented, such as the continued advances in electron tomography and the advent of sensitive elemental detection systems^{1–4}. Furthermore, aberration-corrected transmission electron microscopy has been used to

provide compositional and bonding maps in two dimensions with unprecedented atomic resolution⁵, atomically-resolved tomograms of complete nanoparticles³, and three-dimensional mapping of the orientation of nanoscale grains with a resolution of ~1 nm². However, the study of bulk materials, where features of interest are smaller than the thickness of the specimen (50 to 100 nm), poses a particular challenge in electron microscopy. Since the electron beam must pass through the entire thickness of the specimen, the signal from several overlapping features can become convoluted, making it difficult, and potentially impossible, to accurately interrogate a single specific feature (i.e., a grain boundary, a precipitate, etc.). For example, this is a particular issue in the study of nanocrystalline materials, which are of

current interest due to their unique and unprecedented combinations of properties⁶. It is also the case for alloys with very high volume-fractions of nanometer-scale precipitates or atomic clusters. Additionally, the elemental sensitivity of these techniques, in particular for light elements such as Li, C, or N, generally precludes precise composition measurement.

Atom probe tomography (APT), is an alternative microscopy technique that is capable of generating 3D chemical maps imaging the distribution of individual atoms^{7–8} with near-atomic resolution^{9–12} and, due to the 3D nature of the data, it does not suffer from the limitations noted above. Furthermore, the elemental contrast in electron microscopy scales strongly with atomic number, and hence light elements, which scatter electrons weakly, are difficult to image.

Atom probe tomography is an effective materials characterization technique, complementary to electron microscopy, but which can provide unique microstructural information in its own right. The application of APT has generally been thought of as largely limited to 3D compositional measurements of extremely small features. However, in many APT analyses, crystallographic information has been retained within the data and, importantly, potential applications for this information have recently begun to be recognised^{13–18}. Pioneering research in this area has demonstrated the ability to directly relate the composition of specific microstructural features to their crystallography with unprecedented sensitivity and resolution¹⁹.

Here, after a brief introduction to the fundamentals of atom probe tomography, we review the emerging field of atom probe crystallography, which we define as the analysis and application of crystallographic information within atom probe datasets. This encompasses the observation of atomic planes, the calibration of the tomographic reconstruction, the determination of the orientation of (and orientation relationships between) microstructural features, and orientation mapping in three-dimensions.

Fundamentals of atom probe tomography

Atom probe tomography has developed from field ion microscopy (FIM), the first technique to enable imaging of individual atoms back in the 1950s²⁰. APT exploits the effect of a very intense electric field, on the order of tens of $V\text{nm}^{-1}$, under which the constituent atoms of a material are progressively repelled from the surface and singly or multiply ionized through a mechanism known as field evaporation. Even now the exact theoretical underpinnings of this phenomenon are yet to be totally unravelled^{21–22}. The electric field required to field evaporate an atom is generally called the evaporation field and is specific to each element²³ and phase²⁴ in the material. Conventionally, the field evaporation is triggered by the application of a DC high voltage (HV), which generates around 80 % of the evaporation field. Negative HV pulses are then superimposed by using a counter-electrode placed in front of the specimen. The ions generated are projected from the surface of the specimen and fly towards a position-sensitive detector along trajectories that are initially curved and gradually become almost linear²⁵. The detector collects the ions and records their impact location. The application of voltage-pulsing permits the time-of-flight of each individual ion detected to be measured. Because the time-of-flight is directly related to its mass-to-charge ratio,

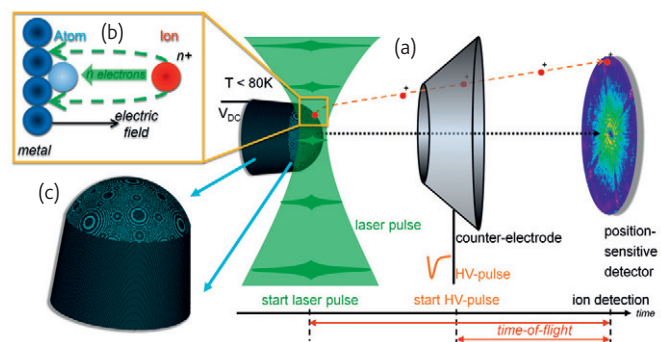


Fig. 1(a) Schematic view of the atom probe microscope. (b) The field evaporation process. (c) Close-up representation of the specimen, here a simple stack of hard spheres on a body-centered cubic lattice. The most protruding atoms at the surface are shown in light blue and form a pattern related to the specimen's crystal structure.

this enables the elemental identification of each detected ion. This process is shown schematically in Fig. 1a-b.

To reach the intense electric fields required by the process, high voltages in the range of a few kilovolts can be used if the specimen is sharpened into the form of a tip with a radius of curvature in the range of 20 to 100 nm. This specimen geometry generates a highly divergent electric field that can be used advantageously as it provides a projection with a magnification of the order of 10^6 , i.e., atoms separated by less than 0.2 nm at the surface of the specimen will strike the detector at locations separated by 0.2 mm, a distance that is easy to differentiate. The impact position on the detector is used to recalculate, with a simple reverse-projection algorithm, the original position of the atom on the specimen surface within the lateral (x-y) plane. Then, by means of a sequential increment of the depth coordinate, a 3D chemically-resolved atom-by-atom reconstruction of the specimen can be progressively built^{26–27}.

Previous instrumentation only allowed the application of APT to the analysis of small and well-distributed features within conductive materials. However, recent technological advances have opened APT to a much broader range of potential applications. The implementation of laser-pulsing capabilities, replacing the conventional HV-pulses, has facilitated application of the technique to non-conductive materials^{28–29}. Laser-pulsing, combined with the large increase in field-of-view permitted by modern microscope designs³⁰ and the capacity for increasingly precise site-specific specimen preparation and analysis^{31–32} has made possible the characterization of a vast array of new nanostructural features. These advances have resulted in a considerable resurgence of interest in APT for the atomic scale investigation of structural and functional materials^{33–36}.

Crystallography in atom probe data

In the image representing an atom probe specimen in Fig. 1c, the atoms highlighted in light blue are the ones that protrude the most from the surface. These atoms are subjected to the most intense electric field and are hence the first atoms to field evaporate in an APT experiment³⁷. It can be seen that they form a pattern of concentric circles. These circles arise due to sets of low-index crystallographic planes that form rings of

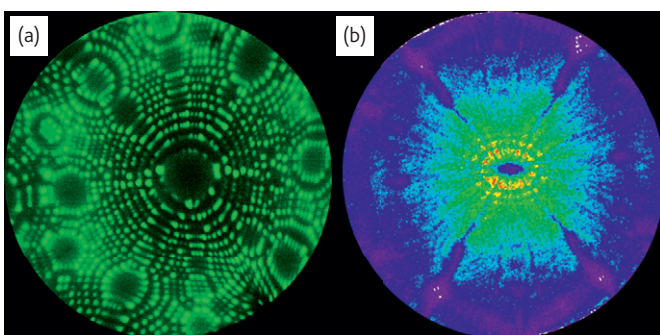


Fig. 2 (a) Digital field ion micrograph of a pure-W specimen oriented along the (110) direction, obtained at 25 K with He used as the imaging gas. (b) Detector hit map (e.g. desorption map) from a pure-W APT analysis obtained at the same temperature and on the same instrument. In (b) the color scales with the local hit-density on the detector, from violet for low-density to red for high-density.

terraces around the corresponding crystallographic direction, called a pole. Zone lines join the facets formed around these poles³⁷. Field ion microscopy highlights the positions of these atoms protruding from the surface. Hence, a typical FIM image, as shown in Fig. 2a, can be interpreted in the same way as the arrangement of protruding atoms in the model of the atom probe specimen in Fig. 1c. The location and shape of crystallographic features in the FIM image are specific to the crystallographic structure of the specimen. From the early 1950s^{20,38} onwards, these elements of crystallography were the first to be interrogated by field ion microscopy.

Images similar to Fig. 2a can be produced via atom probe, although they result from a different physical mechanism. The roughness of the surface associated with poles and zone lines induce subtle inhomogeneities in the electric field distribution very close to the specimen. For example, the electric field is enhanced by 15 to 20 % at the edges of atomic terraces³⁹. These variations are responsible for trajectory aberrations^{40–42}, whereby field evaporated ions are deflected sideways in the early stages of their flight and hence their path to the detector varies slightly. In APT, trajectory aberrations around poles and zone lines translate into regions of high or low hit-density on the detector, as shown on the detector hit-map, also known as a desorption image, presented in Fig. 2b. Local variations of the electric field that provoke aberrations in the ionic trajectories can also arise either from the presence of elements or phases of different evaporation fields, making them easier to identify.

Atomic-resolution imaging with APT

Despite the simplicity of the approach used to produce the tomographic reconstruction, high spatial resolution can still be achieved and facets of the crystallography can be observed within the data. The resolution is high-enough to image individual atomic planes; however, it is not sufficient to directly image the original crystalline lattice of the specimen. A given set of planes can generally be imaged in the reconstructed data in the direct vicinity of the corresponding pole, but cannot necessarily be resolved laterally across the entire reconstruction¹⁶. The imaging of atomic planes requires that during the course of the analysis a steady-state shape of

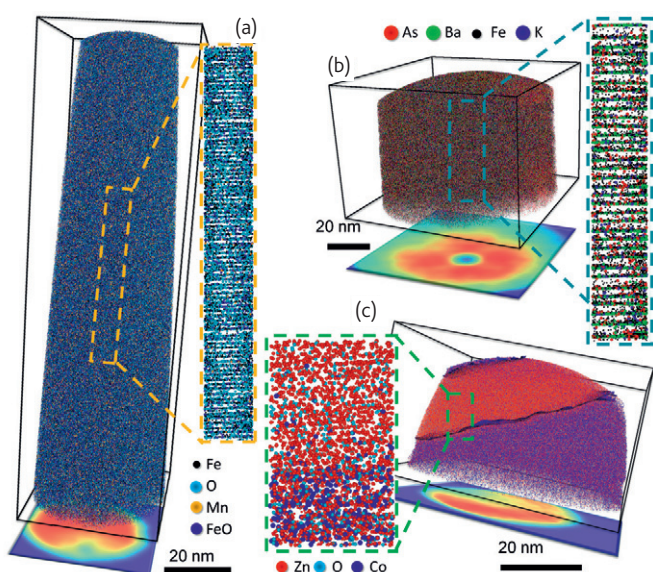


Fig. 3 Atomic planes imaged in various materials that are poor conductors: (a) a thick oxide layer developed on a 316 stainless steel exposed to a Lead-Bismuth Eutectic for 3000 hours at 550°C; (b) a superconductor single-crystal of Fe pnictide ($(\text{Ba}_{0.72}\text{K}_{0.28})\text{Fe}_2\text{As}_2$); (c) ZnO layer in between two layers of Co-doped ZnO . In each case, a two-dimensional density map shown below the reconstructed datasets reveals the presence of a pole in the form of a low density region within the data.

the surface is established⁴³. This in-turn generates a well-defined field evaporation sequence, whereby only atoms from the outermost layer field evaporate⁴³. A high quality evaporation sequence is crucial for layer-by-layer investigation with optimal depth resolution^{10,44–45}.

Initially, atomic planes were imaged in pure metals (W, Al)¹⁸ and in ordered intermetallic phases^{46–47}. For example, imaging atomic planes in several directions enables the identification of variants of ordering in NiAlV alloys⁴⁸, or the reconstruction of the full lattice of the specimen^{49–50}. In highly alloyed systems, large quantities of atoms of different evaporation fields prevent the establishment of a sequence of field evaporation where atoms from the edges of terraces are first to leave the surface, which in turn hinders the imaging of atomic planes. Similarly, in non-conductive materials, the penetration of the electric field within the material is expected to interfere with the field evaporation sequence. However, somewhat unexpectedly, especially for ceramics³⁶ and high-band-gap semiconductors, the presence of atomic planes in the APT reconstruction of these materials is clearly evident in Fig. 3. In these cases, we speculate that imaging atomic planes is enabled by electronic surface states⁵¹ or band bending⁵² that prevents or limits electric field penetration.

Qualification of the tomographic reconstruction

Until recently, the usefulness, and in many cases even the presence of, crystallographic information within atom probe data has largely gone unrecognized. This is mostly due to a lack of practical data-treatment tools enabling the identification and characterization of this information.

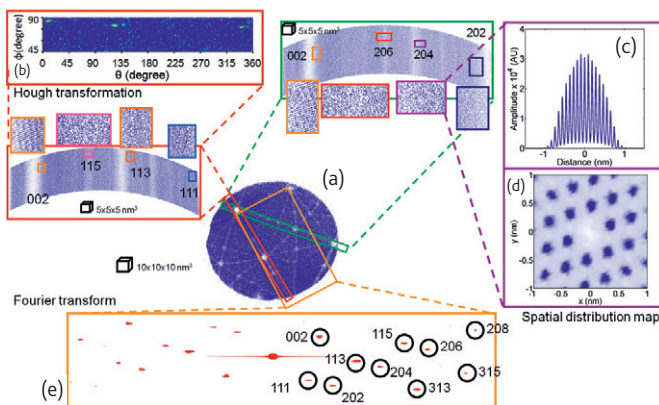


Fig. 4 A pure-Al data set is shown in (a) with close-up views of the multiple atomic plane families imaged within the data. Structural analysis applied to this dataset: (b) Hough transformation in (b), z- and xy-spatial distribution maps respectively in (c) and (d), and Fourier transform in (e).

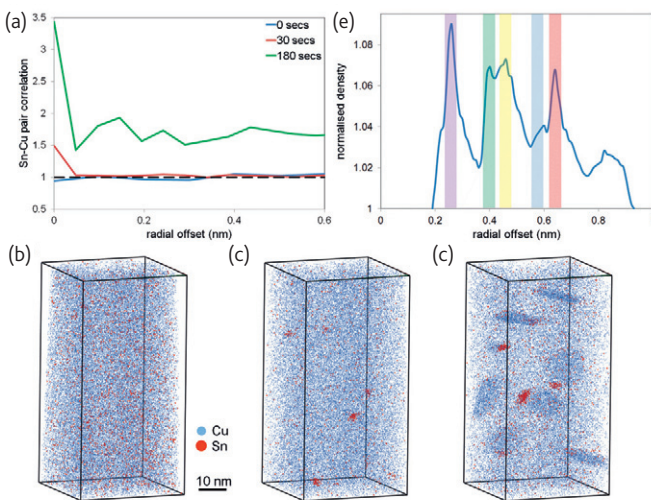


Fig. 5 Radial distribution functions. (a) Pair-correlation function analysis of Cu around Sn atoms in APT analysis of Al-1.7Cu-0.01Sn (at. %) at three stages of thermal treatment at 150 °C: (b) 0 secs (c) 30 secs and (d) 180 secs. A value greater than 1 indicates a positive correlation, i.e. clustering, of Cu with Sn atoms. (e) RDF of atoms in a reconstruction of pure Al. The shaded regions indicate the radii of the first five crystallographic shells in the face-centred cubic Al lattice.

Over the past 15 years, different analytical methods have been developed specifically to this end, including Fourier transform techniques^{12,53-54}, which enable crystallographic characterization in reciprocal space, and, more recently, spatial-distribution maps that are essentially a split radial distribution function^{14,16}, and Hough transforms⁵⁵. The application of these different techniques to a single data set is presented in Fig. 4. The primary

information these tools provide is: (i) the spacing between atomic planes (interplanar spacing), (ii) the angle between sets of planes or directions, (iii) the relative orientation between these planes with respect to the tomographic reconstruction.

The existing method used to build the tomographic reconstruction relies on a set of reconstruction parameters that are linked to both the specimen geometry (radius, shank angle, length, etc.) and local electrostatic environment (distance to the counter electrode, presence of a substrate, etc.). These parameters have long been considered to be constant from specimen-to-specimen²⁶, and rarely have they been appropriately calibrated⁵⁶. However, over the past few years, extensive work has been undertaken to demonstrate how the structural information within atom probe data, although incomplete, can be efficiently used to qualify and calibrate the tomographic reconstruction^{13,16,57-58}. As the global crystallographic structure (body-centered cubic, face-centered cubic, hexagonal close-packed, etc.) of the material under investigation is often known, it is usually possible to constrain and optimize the reconstruction to best match the known-structure⁵⁸⁻⁵⁹. For example, in the dataset presented in Fig. 3 (b), the main pole observed exhibits a 4-fold symmetry characteristic of the (001) direction of the orthorhombic F_{mmn} structure of this Fe-pnictide. Hence the reconstruction parameters were calibrated so as to build a tomographic reconstruction with a planar interspacing in the direction corresponding to the known value of $c/2$ in this material system³⁶. Similar optimization procedures using microstructural features have also been employed to constrain the tomographic reconstruction to reach the appropriate angle between precipitates growing along specific crystallographic directions⁶⁰, or to obtain flat layers or interfaces⁶¹. The development of these calibration procedures represented the first step towards enhanced accuracy of atom probe reconstructions and opened the door to structural analyses.

Investigation of short-range ordering

Short range order is effectively a measure of the likelihood of finding atoms of one specific kind of element, or group of elements, in the near-near vicinity of other atoms of the same type. In many materials design applications it is crucial to understand the specific interactions between the different species so as to control bulk properties. A typical example of this is the inclusion of dopants in semiconductors, which can deactivate when these dopants are distributed too closely together. Conventionally, the existence of short-range order effects has been determined using diffraction-based techniques (electron, neutron and x-ray). However, these approaches face significant disadvantages, such as a limited capacity to detect light elements or atoms of elements at low-concentration and difficulty discriminating elements with similar atomic-numbers. The atomically-resolved 3D data generated by APT is very well suited to interrogation of short-range order and to reveal possible interaction between solutes. The most prominent examples of a type short-range order analyses applied to APT data are cluster-identification algorithms⁶². These algorithms sort mutually-associated atoms into discrete nanostructural features which in turn can be characterized in terms of chemistry, morphology and number density within the system. Frequency distributions of attributes like cluster-size or cluster-chemistry can offer significant qualitative insights into short range order behavior,

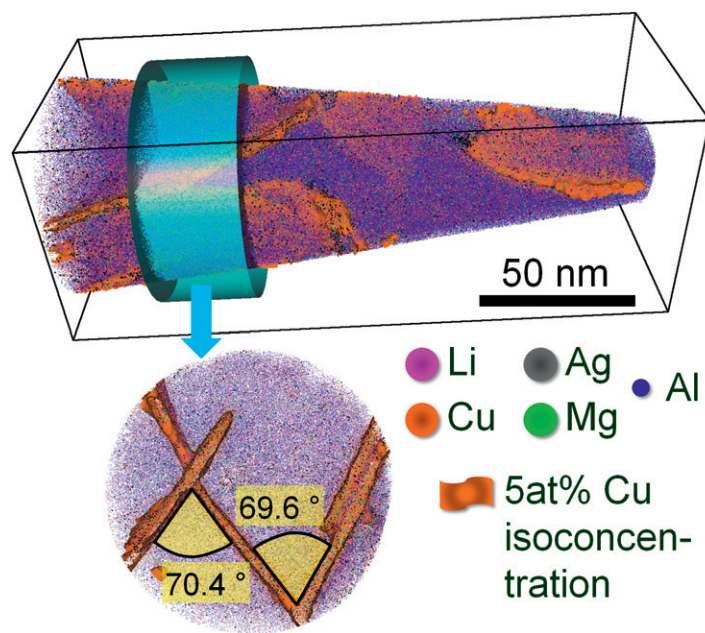


Fig. 6 Atom probe analysis of an Al-Cu-Li alloy containing large T_1 plates that grow along the $\{111\}$ direction. The presence of atomic planes combined with the accuracy of the angles formed between these plates allows for characterization of these precipitates.

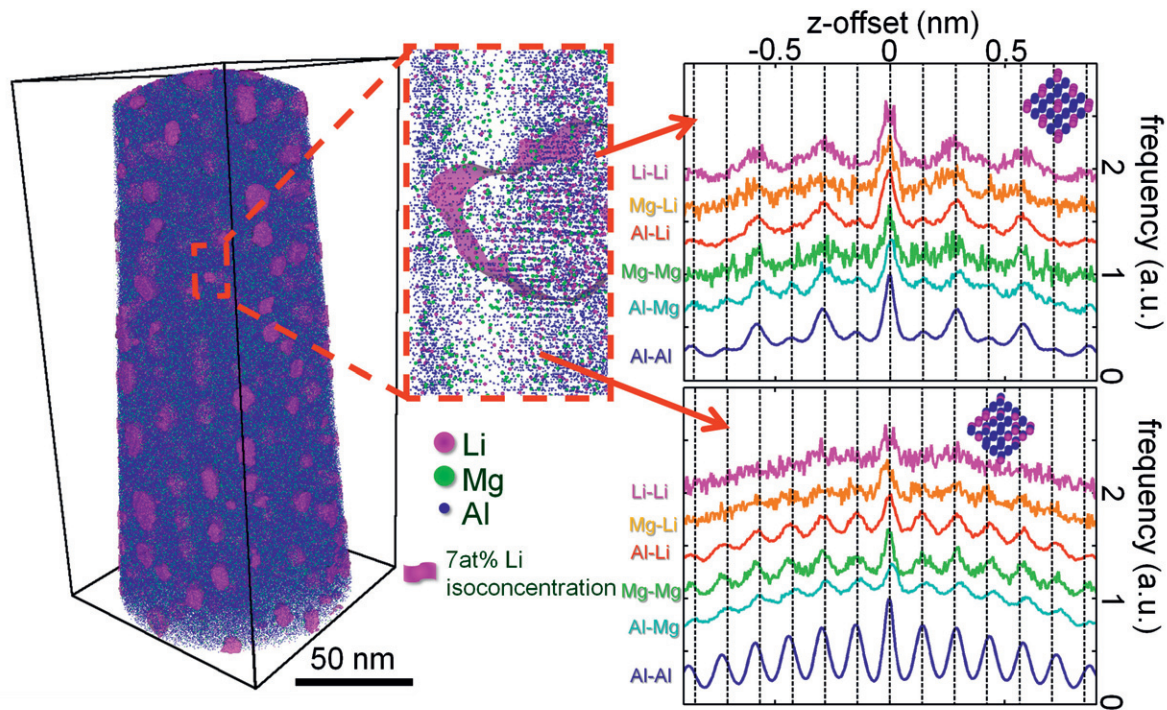


Fig. 7 Tomographic reconstruction from the analysis of an Al-Mg-Li alloy, with an expanded view of a δ' precipitate highlighted by an isoconcentration surface in which the $[022]$ atomic planes are clearly resolved. The spatial distribution maps (right) displayed for atoms in the matrix and the precipitates reveal that Mg partitions to the Li-sites in the ordered precipitates (only 10 % of the Al atoms are displayed).

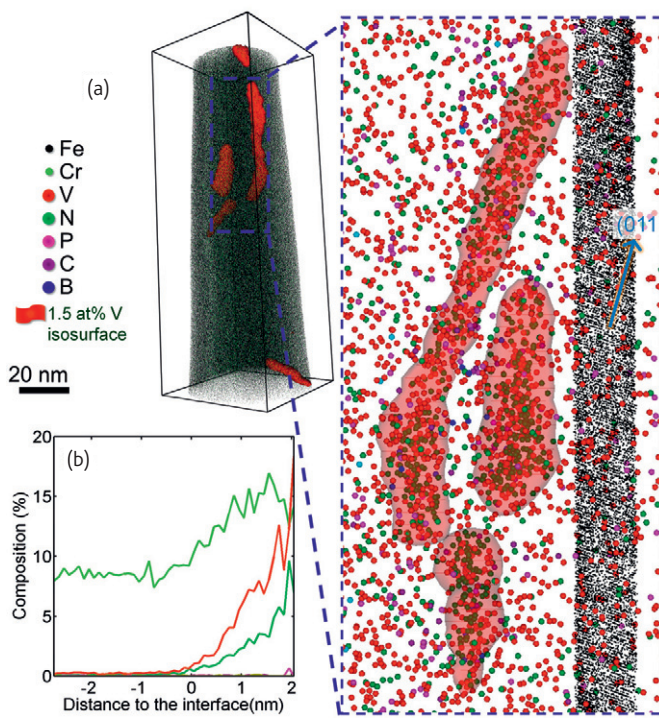


Fig. 8 Chemical segregation of N, V, and Cr around dislocations in a low-activation martensitic steel: (a) three dimensional reconstruction showing the (110) planes and an isoconcentration surface highlighting the segregation in V; (b) composition profile as a function of the distance to this interface (proximity histogram⁵).

particularly when interpreted in comparison to the results obtained from a corresponding randomized model system.

Alternatively, radial distribution function (RDF) analysis is a characterization of the average local arrangement of solute atoms within a solid solution to identify significant spatial- and chemical-correlations^{63,64}. Commonly, the RDF is confined to the analysis of the distribution of a specific element (or elements) in the system to examine the average chemical distribution, termed a partial radial distribution function. Another approach is the pair correlation function, which is similar to the partial-RDF but more specific in its analysis, characterizing the distribution of atoms of a particular element (or group of elements), in the vicinity of atoms of a different element⁶⁵. Fig. 5a shows a pair-correlation function analysis investigating the evolution of the association of Cu around Sn atoms in three early stages in the phase decomposition of an Al-Cu-Sn alloy (Fig. 5b-d)⁶⁶. Identifying the subtle correlation after 30 seconds of ageing in this system would be almost impossible with any other technique.

It has previously been demonstrated that peaks in the RDF analysis of a pure Al APT reconstruction could be observed that corresponded directly to the theoretical pair distances in the face-centered cubic lattice, and this is shown in Fig. 5e⁶⁴. This is an exceptional case and such clear resolution of the lattice in the RDF is uncommon. However, the results of

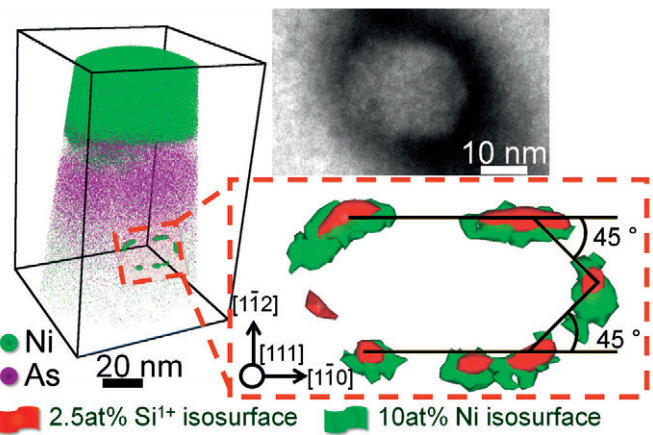


Fig. 9 Chemical segregation imaged around a dislocation loop formed in As-implanted (001) Si. The angle between the loop and specific sets of atomic planes allow for identification of the loop orientation. A loop observed by TEM on a specimen prepared from the same wafer is also presented for comparison (figure re-drawn from ref. ⁸⁵).

the RDF analysis are sometimes interpreted with implicit knowledge of the theoretical crystallography of the system⁶⁷.

Characterization of precipitates and ordered phases

In many materials, energetic and elastic effects favor the precipitation of secondary phases along specific crystalline directions. The introduction of large field-of-view atom probes has made it possible to image large precipitates that have grown along different directions within a single data set. The presence of atomic planes in the tomographic reconstruction and/or poles in the desorption map allows for characterization of the orientation of the precipitates, firstly with respect to the analysis direction, and, more importantly, with respect to a specific crystallographic direction. It has also been demonstrated that in the case where atomic planes are not imaged but precipitates with specific compositions and a known relative orientation (pre-determined by electron microscopy for example) are observed then the angle formed between these precipitates can be used to calibrate the reconstruction⁶⁰. A typical example is shown in Fig. 6 where several T₁ plates from an Al-Cu-Li alloy (AA2198) heat treated for 100 h at 155 °C were observed. These precipitates are known to form along the {111} direction of the Al-fcc matrix. Here, the reconstruction was calibrated using the methodology introduced in ref.^{13,58} based on the location of the poles that appear within the matrix region of the desorption map and to optimize the interplanar spacing of the [111] planes. The angle between the plates is approximately 70 degrees, in good agreement with the expected value. This capacity of atom probe tomography to investigate the crystallographic relationship between particles or precipitates and the surrounding matrix has only recently been recognized and utilized and there is much potential for combining the compositional information with the crystallographic information available for the identification and characterization of different phases and intra-granular precipitates and particles.

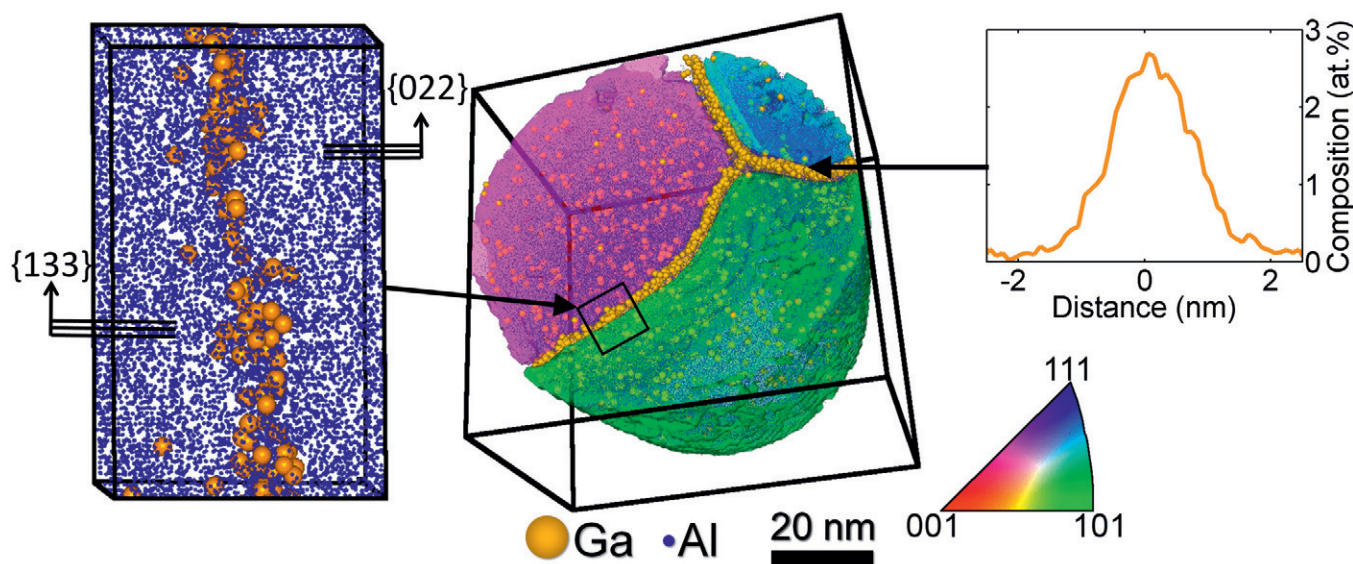


Fig. 10 Atom probe orientation mapping in a nano-crystalline aluminium thin-film highlighting the segregation of Ga at the grain boundary. The zoomed in image on the left of the reconstructed volume shows that the imaged atomic planes extend up to the grain boundary and the graph on the right is a proximity histogram highlighting the extent of the segregation at the grain boundary. The grains in the central image are coloured according to their orientation, as indicated by the inverse pole figure.

Other aspects of the fine structure of precipitates can be investigated by exploiting the crystallographic information present within atom probe data. In some alloy systems, atoms display long range ordering, arranging themselves into periodic patterns that span the entire crystal. Ordered phases appear in intermetallic systems (e.g., FeAl, Ni₃Al, etc.). These phases adopt structures in which the atoms of different elements preferentially occupy specific sites on the lattice with respect to the relative positions of one another. The capacity of atom probe tomography to analyze individual atomic planes has been exploited to reveal which sub-lattice was occupied by trace or alloying elements^{14,46-47,68-69}. Such analysis has generally been the domain of advanced electron microscopy or diffraction techniques⁷⁰. However, in some systems, ordering can be very difficult to identify, for example where a large population of small precipitates form in a matrix and the atoms are either light or of comparable atomic number. Previously, structural information has not been obtainable from such small features in APT reconstructions since the statistics available within an individual precipitate were not sufficient to resolve a signal in the SDM of a Fourier transform analysis. However, recently an approach was developed whereby the precipitates were isolated from the matrix and subsequently a single SDM analysis was applied that incorporates contributions from all of the precipitate atoms within a region of interest⁷¹. By combining the contributions from many small precipitates the ordering of the structure could be determined by the SDM analysis.

An example is shown in Fig. 7, where an Al - 5 wt% Mg - 1.8 wt% Li alloy has been aged for 8 hours at 150 °C and a large volume fraction of δ' precipitates have formed. Similar precipitates with an Al₃Li stoichiometry form in an Al-Li binary alloy and adopt a L1₂-type structure, which means that the Li occupies the edges of the cube in a face-centered cubic crystal, while the Al occupies the center of the faces⁷². It was not known if the

additional Mg atoms would partition to the Al- or Li-sites. The application of element-specific (or partial) spatial distribution map techniques reveals significant structural information. Firstly, it is apparent that precipitates are indeed ordered, as there is a clear change in periodicity of the distribution of the elements along the [022] direction within the precipitates compared to within the matrix. Secondly, these partial spatial-distribution maps also reveal that in the matrix, Mg and Li indifferently occupy any site, however, in the precipitates, peaks corresponding to the Mg-Mg Li-Li and Mg-Li distributions appear with double-spaced periodicity, indicating that the Mg occupies the Li-lattice⁷¹. This long-standing question could only be answered through the application of atom probe crystallography techniques⁷³. It is worth noting that the accuracy of this measurement is limited by the preferential evaporation of the Mg and Li from the precipitates⁷⁴.

Crystalline defects

Since its inception, field ion microscopy has often been used to investigate crystalline defects such as individual vacancies⁷⁶ or dislocations and dislocation loops^{77,78}. A particularly significant contribution was the investigation of vacancies caused by radiation damage in metals⁷⁹. Although these crystalline defects cannot be directly imaged by atom probe tomography due to a combination of limited spatial resolution and detection efficiency, chemical segregation at defects is routinely observed in APT reconstructions. For example, the first evidence of Cottrell atmospheres was provided by atom probe analyses of intermetallics⁸⁰ where, because atomic planes were imaged intersecting this feature, the presence of the dislocation could be directly evidenced. Since this world-first, similar segregation effects have been imaged and characterized in a wide variety of systems⁸¹, particularly in steels^{82,83}, as shown in Fig. 8,

and in Si-based semiconductors, where they are observed in the form of dislocation loops^{34,84-85} or dislocations caused by radiation damage⁸⁶, as shown in Fig. 9a-b. Advances in the crystallographic analysis of atom probe data enable the accurate characterization of the orientation of the dislocation loop by identifying the angles between the plane containing the loop and sets of atomic planes of well-known crystallographic orientations.

Grain boundary misorientation and orientation mapping

Materials fabricated or processed in order to obtain an average grain-size on the order of only a few tens-of-nanometers have been shown to exhibit exceptional properties^{15,87,88}. However, atomic-scale characterization of such materials by conventional methods can be extremely challenging. As mentioned in the introduction, beam-based microscopy techniques suffer from intrinsic limitations associated with the small size of the features of interest with respect to the thickness of the samples, such as for the case of the analysis of individual grain boundaries in nanocrystalline alloys. This case, as shown in Fig. 10, is an example of a type of analysis where the 3D nature of the APT data provides a real advantage by allowing the precise measurement of the local distribution of atoms at specific locations within these materials.

Significantly, the orientation of each individual grain within a given data set can be determined with respect to the analysis direction thanks to the capacity to identify, index, and characterize the orientation of crystallographic poles in the reconstruction. This allows for three-dimensional orientation mapping, similar to that obtained by using a combination of electron-backscattered diffraction (EBSD) and FIB slice-and-view⁸⁹⁻⁹⁰, but on a much smaller scale. Furthermore, in cases where three sets of atomic planes can be visualized in more than one grain, the relationship between the crystallographic orientation of the two grains can be accurately determined^{17,91}, where this relationship can be expressed as the grain boundary disorientation, or the smallest rotation angle between neighboring grains. The use of atom probe tomography enables these measurements to be performed at a much finer scale, down to grains that are only a few nanometers in size. The three-dimensional nature of the data also provides other insights into the structure of the material. For example, it is possible to extract information about the local roughness of an interface^{92,93} or the curvature of a grain boundary¹⁵, which can then be directly correlated to both the local concentration and the boundary disorientation.

Remaining issues and future developments

Applications for atom probe crystallography are only just being recognized and the potential is enormous. For example, Ceguerra et al. have recently adapted an approach for the measurement of short-range order parameters in APT data⁹⁴. A complete set of short-range order parameters provides a comprehensive description of the average arrangement of atoms in the system. It should be noted that the short-range order parameters measured from an APT data are limited by the spatial resolution limits and various artifacts that are inherent to every reconstruction. No experiment has yet been undertaken to investigate how well these values reflect those obtained by more conventional

scattering approaches, but the accuracy is likely to be strongly system dependent. Nevertheless, the short-range parameters comprise highly valuable information. It was recently demonstrated that these parameters can be used as target values in a Monte Carlo algorithm to generate an equivalent yet lattice-based and complete simulated system. Further, this approach is highly complementary to another emerging technique; lattice rectification. In lattice rectification the arrangement of atoms in an APT reconstruction is restored to the perfect lattice configuration of the original system by characterizing and utilizing the existing incomplete crystallographic structure within the data⁴⁹⁻⁵⁰. The combination of short-range order based Monte Carlo techniques and lattice rectification raises an intriguing prospect, the capacity to replace the atoms missing due to detection-efficiency limitations in the current generation of atom instruments. Lattice-based and completed APT reconstructions could be seeded directly into a range of simulations and modeling approaches providing a radical new approach to the way nanostructure-property relationships are investigated.

It is important to note that the amount and quality of the crystallographic information that are retained depend on the analyzed material and that atom probe crystallography may not be amenable to every single dataset or even specimen to be analyzed. Nonetheless, the unique insights brought by this technique make it worth developing further. Improvement to the approach for reconstruction is critical to future progress of atom probe crystallography. Steady advances continue to be made in the development of the current protocol^{26-27,57} but it still remains too simple to account for complex tip shapes observed experimentally^{95-97,98} that cause trajectory aberrations. The complex flight-path taken by the ions can, in theory, be modeled based on electrostatic simulations^{42,98-99}, but as pointed out by Haley *et al.*⁹⁸, this process is not straightforward as there is no unique solution. Additional constraints should be imposed to minimize the possible solutions, for example by using additional information gained from electron tomography^{98,100}, but the applicability of such methodology and its potential efficacy remain to be demonstrated. The crystallographic details already present within atom probe data can be used directly to derive the best possible reconstruction^{13,58-59}. The inevitable automation of these new methods will create an extremely powerful microscopy tool that is set to make a very large impact on materials science. **mt**

Acknowledgements

The authors are grateful for scientific and technical input and support from the Australian Microscopy & Microanalysis Research Facility (AMMRF) at The University of Sydney. The oxidized stainless steel was provided by Drs P. Hoseman and E. Stergar from UC Berkeley. The low-activation steel is a CLAM (HEAT-0912) steel provided by FDS team, Institute of Plasma Physics, Chinese Academy of Sciences. The AlMgLi alloy was provided by Prof. A. Deschamps, Université Joseph Fourier Grenoble, France. The nano-crystalline Al sample was provided by Prof. D. Gianola, University of Pennsylvania, and the data acquired at the ACMM by Dr F. Tang. Datasets shown in Figure 9 were provided by Dr K. Hoummada, IM2NP, Marseille, France. All other datasets were acquired at the ACMM: the Fe-pnictide dataset by Dr. W. Yeh; the Co-doped ZnO by Mrs L. Li; the AlCuSn alloy was provided by Dr T. Homma, Nagaoka University.

References:

1. Midgley, P. A., and Dunin-Borkowski, R. E., *Nat Mater* (2009) **8**(4), 271.
2. Liu, H. H., et al., *Science* (2011) **332**(6031), 833.
3. Van Aert, S., et al., *Nature* (2011) **470**(7334), 374.
4. Collieux, C., *Nature* (2007) **450**(29), 622.
5. Muller, D. A., *Nature Materials* (2009) **8**(4), 263.
6. Arzt, E., *Acta Materialia* (1998) **46**(16), 5611.
7. Blavette, D., et al., *Nature* (1993) **363**(6428), 432.
8. Seidman, D. N., and Stiller, K., *MRS Bulletin* (2009) **34**(10), 717.
9. Cadel, E., et al., *J Appl Phys* (2009) **106**(4), 044908.
10. Gault, B., et al., *Appl Phys Lett* (2009) **95**(3), 034103.
11. Gault, B., et al., *Microsc Microanal* (2010) **16**, 99.
12. Vurpillot, F., et al., *J Microscopy* (2001) **203**, 295.
13. Gault, B., et al., *Microsc Microanal* (2008) **14**(4), 296.
14. Geiser, B. P., et al., *Microsc Microanal* (2007) **13**(6), 437.
15. Liddicoat, P. V., et al., *Nature Communications* (2010) **1**, 63.
16. Moody, M. P., et al., *Ultramicroscopy* (2009) **109** 815.
17. Sha, G., et al., *Ultramicroscopy* (2011) **111**(6), 500.
18. Warren, P. J., et al., *Ultramicroscopy* (1998) **73**(1-4), 261.
19. Araullo-Peters, V., et al., *Scripta Mater* (2012) **66**(11), 907.
20. Müller, E. W., *J Appl Phys* (1956) **27**(5), 474.
21. Kreuzer, H. J., et al., *Phys Rev B* (1992) **45**(20), 12050.
22. Forbes, R. G., *Appl Surf Sci* (1994) **87/88**, 1.
23. Brandon, D. G., *Philosophical Magazine* (1966) **14**(130), 803.
24. Ge, X. J., et al., *J Appl Phys* (1999) **85**(7), 3488.
25. Smith, R., and Walls, J. M., *J Phys D-Appl Phys* (1978) **11** (4), 409.
26. Bas, P., et al., *Appl Surf Sci* (1995) **87-88**, 298.
27. Gault, B., et al., *Ultramicroscopy* (2011) **111**(6), 448.
28. Gault, B., et al., *Rev Sci Instrum* (2006) **77**, 043705.
29. Kelly, T. F., and Miller, M. K., *Rev Sci Instrum* (2007) **78**, 031101.
30. Kelly, T. F., et al., *Microsc Microanal* (2004) **10**(3), 373.
31. Thompson, K., et al., *Ultramicroscopy* (2007) **107**(2-3), 131.
32. Feifer, P., et al., *Ultramicroscopy* (2011) **111** (6), 435.
33. Perea, D. E., et al., *Nature Nanotechnology* (2009) **4** (5), 315.
34. Thompson, K., et al., *Science* (2007) **317** (5843), 1370.
35. Tedsree, K., et al., *Nature Nanotechnology* (2011) **6** (5), 302.
36. Yeoh, W. K., et al., *Phys Rev Letters* (2011) **106**, 247002.
37. Moore, A. J. W., *J Phys and Chemistry of Solids* (1962) **23** (JUL), 907.
38. Chen, Y. C., and Seidman, D. N., *Surface Science* (1971) **26** (1), 61.
39. Vurpillot, F., Etude de la fonction de transfert pointe-image en sonde atomique tomographique. PhD thesis, The Uniservity of Rouen, Rouen, 2001.
40. Waugh, A. R., et al., *Surface Science* (1976) **61**, 109.
41. Miller, M. K., and Hetherington, M. G., *Surface Science* (1991) **246**, 442.
42. Vurpillot, F., et al., *Appl Phys Lett* (2000) **76** (21), 3127.
43. Gruber, M., et al., *Surface Science* (2011) **605** (23-24), 2025.
44. Vurpillot, F., et al., *Ultramicroscopy* (2000) **84** (3-4), 213.
45. Gault, B., et al., *J Appl Phys* (2010) **108**, 044904.
46. Blavette, D., et al., *Comptes rendus de l'Academie des sciences. Serie 2, Mecanique, physique, chimie, sciences de l'univers, sciences de la terre.* (1993) **317** (10), 1279.
47. Blavette, D., and Menand, A., *MRS Bulletin* (1994) **19** (7), 21.
48. Marteau, L., et al., *J Microscopy* (2001) **204**, 247.
49. Vurpillot, F., et al., *Ultramicroscopy* (2003) **95** (1-4), 223.
50. Moody, M. P., et al., *Microsc Microanal* (2011) **17** (2), 226.
51. Vella, A., et al., *J Appl Phys* (2011) **110** (4), 044321.
52. Tsong, T. T., *Ultramicroscopy* (1979) **4** (3), 389.
53. Warren, P. J., et al., *Microsc Microanal* (1998) **5**, 89.
54. Vurpillot, F., et al., *J Microscopy-Oxford* (2004) **216**, 234.
55. Yao, L., et al., *Ultramicroscopy* (2011) **111** (6), 458.
56. Hyde, J. M., et al., *Appl Surf Sci* (1994) **76/77**, 382.
57. Gault, B., et al., *Ultramicroscopy* (2011) **111** (11), 1619.
58. Gault, B., et al., *J Appl Phys* (2009) **105**, 034913.
59. Larson, D. J., et al., *Microsc Microanal* (2011) **17** (SupplementS2), 724.
60. Gault, B., et al., *Ultramicroscopy* (2011) **111** (6), 683.
61. Larson, D. J., et al., *J Microscopy* (2011) **243** (1), 15.
62. Marquis, E. A., and Hyde, J. M., *Materials Science and Engineering: R: Reports* (2010) **69** (4-5), 37.
63. Sudbrack, C. K., et al., *Phys Rev B* (2006) **73** (21), 4.
64. Haley, D., et al., *Philosophical Magazine* (2009) **89** (11), 925.
65. De Geuser, F., et al., *Philosophical Magazine Letters* (2006) **86** (4), 227.
66. Homma, T., et al., *Metallurgical and Materials Transactions A* (2012) in press (DOI: 10.1007/s11661-012-1111-y).
67. van Dalen, M. E., et al., *Acta Materialia* (2011) **59** (20), 7615.
68. Miller, M. K., and Horton, J. A., *Scripta Metallurgica* (1986) **20** (8), 1125.
69. Yamamoto, M., and Seidman, D. N., *Surface Science* (1983) **129** (2-3), 281.
70. Taftø, J., and Spence, J. C. H., *Science* (1982) **218** (4567), 49.
71. Gault, B., et al., *Scripta Mater* (2012) **66** (11), 903.
72. Rossell, M. D., et al., *Phys Rev B* (2009) **80** (2), 024110.
73. Thompson, G. E., and Noble, B., *Journal of the Institute of Metals* (1973) **101** (APR), 111.
74. Blavette, D., et al., *Ultramicroscopy* (1998) **70** (3), 115.
75. Hellman, O. C., et al., *Microsc Microanal* (2000) **6** (5), 437.
76. Seidman, D. N., *Bulletin of the American Physical Society* (1972) **17** (3), 362.
77. Brandon, D. G., and Wald, M., *Philosophical Magazine* (1961) **6** (68), 1035.
78. Fortes, M. A., et al., *Philosophical Magazine* (1968) **17** (145), 169.
79. Scanlan, R. M., et al., *Philosophical Magazine* (1971) **23** (186), 1439.
80. Blavette, D., et al., *Science* (1999) **286** (5448), 2317.
81. Jayaram, R., and Miller, M. K., *Scripta Metallurgica Et Materialia* (1995) **33** (1), 19.
82. Wilde, J., et al., *Scripta Mater* (2000) **43** (1), 39.
83. Xie, K. Y., et al., *Scripta Mater* (2012) **66** (9), 710.
84. Duguay, S., et al., *Appl Phys Lett* (2010) **97**, 242104.
85. Hoummada, K., et al., *Scripta Mater* (2011) **64** (5), 378.
86. Etienne, A., et al., *J Nucl Mater* (2010) **406** (2), 244.
87. Gleiter, H., et al., *Acta Materialia* (2001) **49** (4), 737.
88. Tang, F., et al., *Acta Materialia* (2012) **60** (3), 1038.
89. Xu, W., et al., *Materials Characterization* (2007) **58** (10), 961.
90. Xu, W., et al., *Acta Materialia* (2007) **55** (15), 5157.
91. Moody, M. P., et al., *Ultramicroscopy* (2011) **111** (6), 493.
92. Larson, D. J., et al., *Acta Materialia* (1999) **47** (15-16), 4019.
93. Larson, D. J., et al., *Acta Materialia* (2004) **52** (10), 2847.
94. Ceguerra, A. V., et al., submitted to *Acta Crystallographica A* (5/07/2011) (2012).
95. Bolin, P. L., et al., *J Phys E-Scientific Instruments* (1976) **9**, 363.
96. Vurpillot, F., et al., *Surface and Interface Analysis* (2004) **36** (5-6), 552.
97. Marquis, E. A., et al., *J Microscopy* (2011) **241** (3), 225.
98. Haley, D., et al., *J Microscopy* (2011) **244** (2), 170.
99. Oberdorfer, C., and Schmitz, G., *Microsc Microanal* (2011) **17** (01), 15.
100. Arslan, I., et al., *Ultramicroscopy* (2008) **108** (12), 1579